Chapter 2 – INSTRUMENTATION

2.1 THE IONOSONDE

(John MacDougall, Dept. of Electrical and Computer Engineering, University of Western Ontario, London, Ont. Canada N6A 5B9)

2.1.1 Ionospheric Sounding

An Ionosonde is an HF radar used for obtaining electron density profiles of the ionosphere. It basically works on the principle that a radio wave will be totally reflected if the radio frequency is equal to the characteristic frequency of the ionosphere which depends on plasma frequency, $f_p = (80.5N)^{1/2}$ Hz, where N is the electron density in electrons per m^3. Thus knowing the height of reflection and the radio frequency one has a measurement of the electron density at that height.

This simplified principle is somewhat more complex in practice since the group velocity of the radio wave is slower in the ionosphere so the height obtained using the time delay of the echo and assuming that the radio wave travels at the speed of light is an overestimation of the actual height of reflection. Also, the ionosphere is birefringent for radio waves so that the reflection conditions for one mode, the extraordinary wave, are different from the reflection conditions for the other mode, the ordinary wave. The electric field of the ordinary wave is left hand circularly polarized when viewed along the direction of the terrestrial magnetic field. For ordinary waves the reflection condition is simple in that the wave is reflected at the level where the frequency just equals the plasma frequency as defined above. It is therefore necessary to have a way of separating out the ordinary wave reflections when calculating ionospheric densities from the echoes obtained by an ionosonde. Having separated out the O mode echoes an estimation of the electron density profile can be obtained using a "true height analysis" program. The best known true height analysis program is Polan [Titheridge, 1985, 1998].

2.1.2 Ionosonde Specifications

From these, and other, considerations one can list the specifications for an ionosonde:

1) **Frequency Range:** Based on maximum ionospheric densities up to a few times 1.0×10^{12} electrons per m^3 => 9 MHz plasma frequency. Thus ionosondes that will be used for obtaining overhead electron densities typically should have an upper frequency ~20 MHz. The minimum frequency is generally determined by considerations such as antenna size, licensing restrictions, and ionospheric absorption effects (higher at low frequencies). Minimum ionosonde frequencies of the order of 1 MHz are typical.

2) **Range:** Since an ionosonde can only obtain echoes where its frequency matches the plasma frequency it is limited to observations of the 'bottomside' of the ionosphere. (When it uses a frequency higher than the maximum plasma frequency of the ionosphere the transmitted pulse passes through the ionosphere without reflection.) The height range of interest is therefore from about 90 kilometers up to the order of 1000 km.

3) **Range Resolution:** If the ionosonde is just being used for electron density profiles then range resolution of a few kilometers is usually adequate since it is only when there is Sporadic E present that there is major ionospheric structure with a scale size smaller than a few kilometers. Note that high range resolution implies shorter pulses and therefore wider receiver bandwidth and hence higher receiver noise levels. For this reason most ionosondes are not designed to have range resolution better than a few kilometers.

4) **Polarization Separation:** Some way of separating O and X circular polarization is necessary. This can be done by using antenna arrangements, and electronics, that only transmit the O or X mode. An alternative method is to combine signals from perpendicularly orientated receiving antennas in such a way that the two modes of the echoes can be determined. Of course visually one can usually distinguish between the O and X modes because the X mode is reflected with about ½ electron gyrofrequency (typically ~1/2*1.4 MHz) higher frequency than the O mode.

5) **Transmitter Power:** Older model ionosondes used large peak transmitter power of the order of 10 kW [Hunsucker, 1991]. This was necessary in order to get acceptable signal-to-noise performance. Newer ionosondes generally use some form of signal coding/processing to improve the signal-to-noise.

The following is a basic calculation of the signal-to-noise pertinent to an ionosonde. At HF the noise levels on the ground are very high. There are also other users on these frequencies which make the noise situation even worse. For this calculation an average noise temperature of 10^8 K will be used. Assuming a 30 kHz receiver bandwidth (typical ionosonde value) the received noise power would be 4×10^{-11} W. If a signal-to-noise ratio of 20 dB is required then the received power should be 4×10^{-9} W. The received power for a transmitted power P_T is $P_R = P_T\, G_T\, G_R\, \lambda^2 /(4\pi R)^2$ where G_T is the gain of the transmitter antenna, G_R is the gain of the receiver antenna, λ is the wavelength, R is the range which for specular (total) reflection is twice the actual range. (If there is ionospheric absorption of the signal the power received would be lower.) For calculation use: $G_T = G_R = 1$, $\lambda = 100$ m, $R = 2\times300$ km and from these obtain a required $P_T = 23$ W. Thus, theoretically, an ionosonde requires only very low peak transmitter power even without coding/signal processing.

In general, ionosondes use very much higher peak power than 23 W. There are a number of reasons for this. The most obvious reason is that the gains of the transmitting and receiving antennas are usually much less than 1. This is because it is expensive to build wideband HF antennas that have an upward pointing beam and have good gain. Assuming that the antenna gains are only 1/10 then the peak power required becomes 2.3 kW which is comparable with the 10 kW power used for older ionosondes.

Because it is easy to obtain power levels of a few hundred watts using solid state amplifiers, and it is convenient and inexpensive to do digital coding/signal processing, most modern ionosondes have peak power of the order of 100-1000 W and employ a great deal of coding/signal processing techniques. As a typical example, using 13 bit Barker code the signal-to-noise is improved by $10\times\log(13) = 11$ dB, and employing coherent (FFT) averaging on 8 samples gives another 9 dB so a total improvement of 20 dB is easily obtained. One could obtain further improvement by using a longer code [Huang and MacDougall, 2005] but the requirement to obtain echoes from a height of ~90 km means that the total length of the coded pulse cannot be longer than ~600 μs unless the transmitter and receiver are located sufficiently far apart that the transmitted pulse will not saturate the receiver.

Further signal-to-noise improvement can be obtained by coherently averaging a number of samples. The signal-to-noise improvement is 10*log(number of samples). However there is a problem in this if there is an appreciable Doppler shift in the received echoes since, for a long series of samples, the phase shift of the later samples, relative to the first samples, could become sufficiently large that when one coherently adds them they might subtract rather than add. It is of course possible to overcome this problem by progressively phase shifting the samples to remove the Doppler phase shifts. The problem with doing this is that one does not know a value for the Doppler shift. However, one can get around this problem by doing an FFT instead of coherent averaging. An FFT is effectively the same, if one chooses the correct frequency bin, to removing the Doppler phase shifts by progressively phase shifting the samples before coherently averaging them. This means that at least theoretically, one can use as large a number of samples for the FFT as desired for signal-to-noise improvement. Usually the number of samples is curtailed by the desire to minimize the time needed to obtain the echo results for each ionosonde frequency. A good discussion of some of these signal

processing techniques as used in ionosondes is the Digisonde web site [http://ulcar.uml.edu/digisonde_dps.html]. See also Reinisch [1996]. There is an abundance of additional information about ionosondes on the Internet.

2.1.3 Ionogram Samples

The behaviour, and hence ionogram appearance, of the earth's ionosphere are different for different locations. A simplified division of the regions showing different ionogram behaviour are: mid-latitudes, auroral zone, polar cap region, equatorial region. A few examples from these regions are shown here.

Figure 2-1 shows samples of ionograms from Delaware (43° N, 81° W) for 2006 September 8. Times marked are UT: subtract 5 hours for local time. Daytime ionograms are shown in the two left hand panels, and nighttime in the two right hand panels. In daytime sunlight directly creates the F_1 layer. Above the F_1 layer one sees the F_2 layer which essentially is due to the reduction of recombination at greater heights. There is also a weak E region, also sunlight produced. During daytime echoes, particularly on lower frequencies, may be weak due to radio wave absorption in the lower D region. After sunset the F_1 layer disappears and a progressively weaker F_2 layer remains throughout the night, as seen in the two nighttime panels.

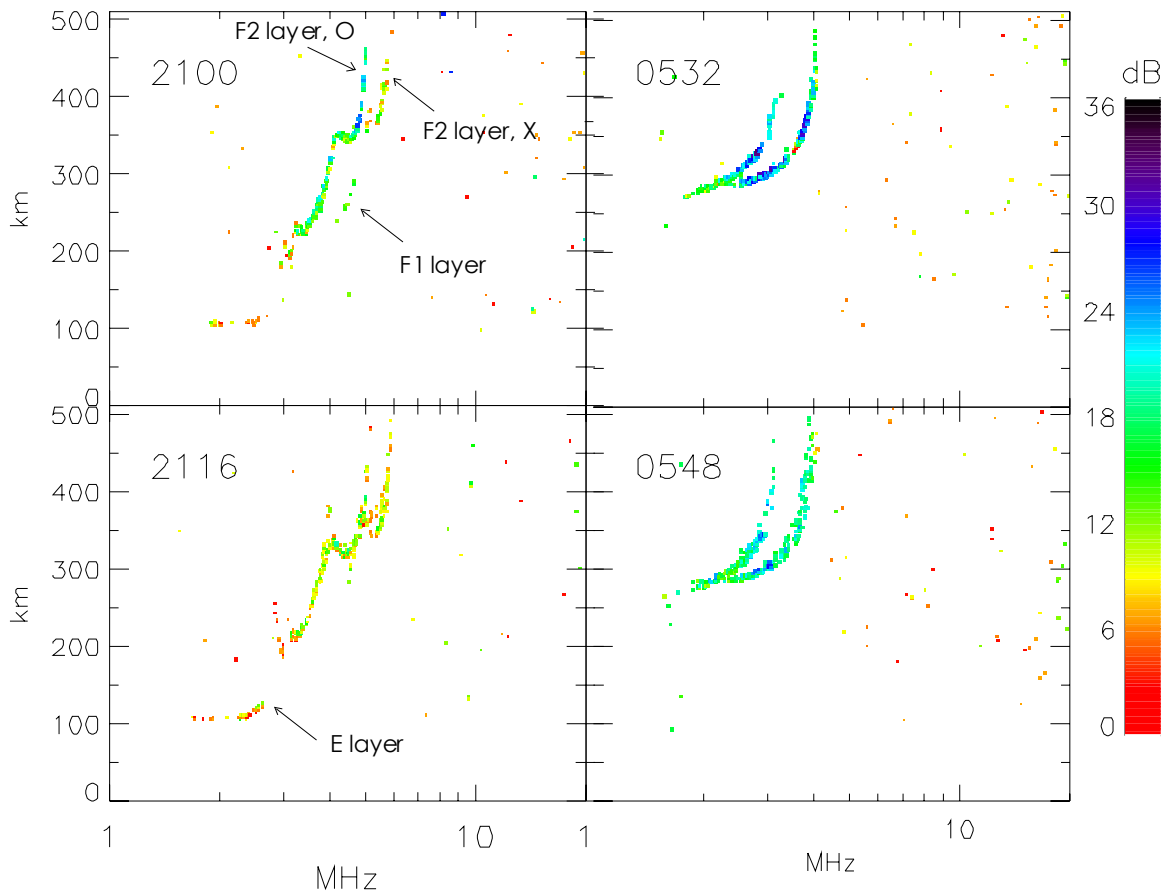

Figure 2-1: Mid-Latitude Ionograms.

Figure 2-2 shows ionograms from Rabbit Lake (58°N, 104°W) for early nighttime 1995 Nov. 8. For these ionograms one sees E region (heights 90 – 150 km) echoes from a layer that is created by energetic precipitation. The appearance of the layer varies notably between the samples. Sometimes one sees a thick

layer (as at 0200) with the O and X traces being distinguishable, whereas at other times one just sees an irregular patch. If the precipitation becomes very energetic it creates a D region below 90 km and this absorbs the radio signals so the ionogram may not show any sign of echoes.

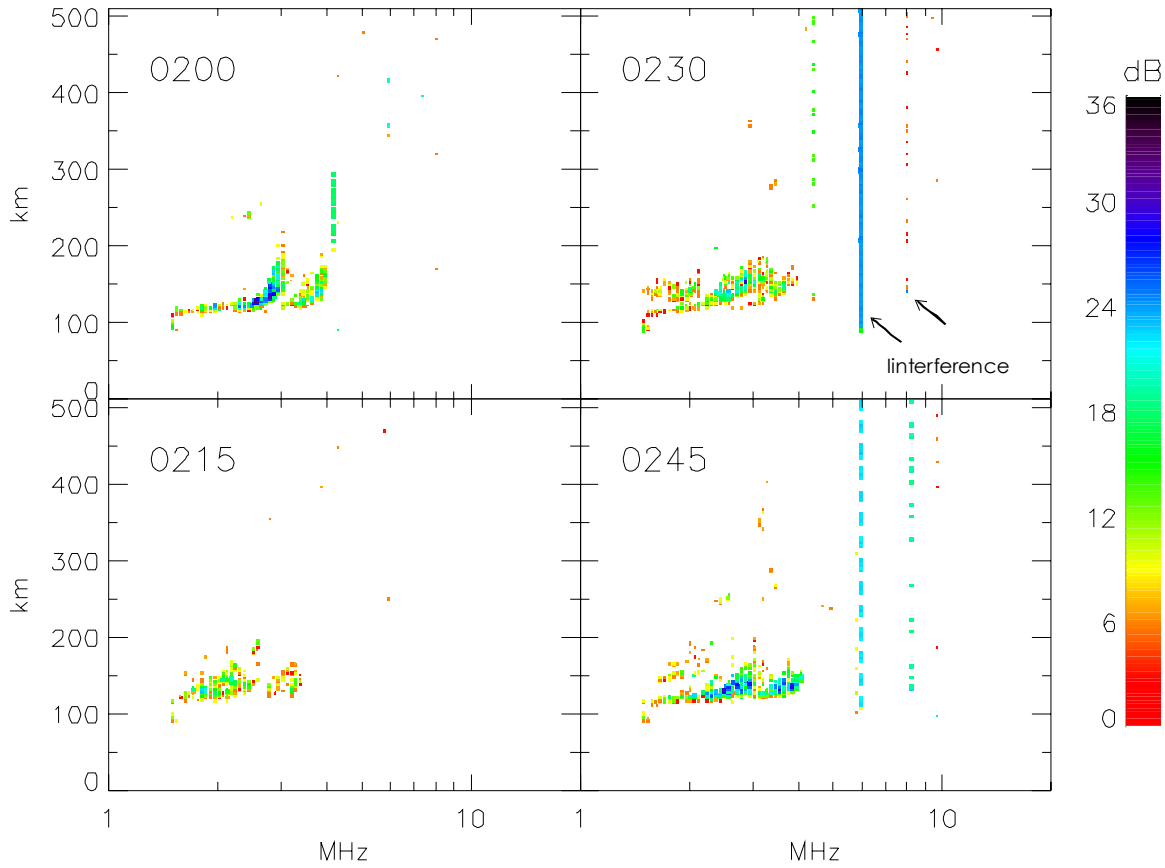

Figure 2-2: Auroral Zone Ionograms.

Figure 2-3 shows ionograms from Resolute Bay, 2007 January 8. Times in UT are marked on the ionograms. Resolute Bay (75° N, 95° W) is in the polar cap region. Note the spreading which is typical for polar cap ionograms. On only one of the 4 ionograms can one clearly distinguish the Ordinary (O) and Extraordinary (X) traces. Other features such as Sporadic-E (Es), vertical interference streaks, off vertical (non overhead) echoes, and 2nd hop echoes (reflected from ionosphere and then from ground and back to 2nd ionospheric reflection) are marked.

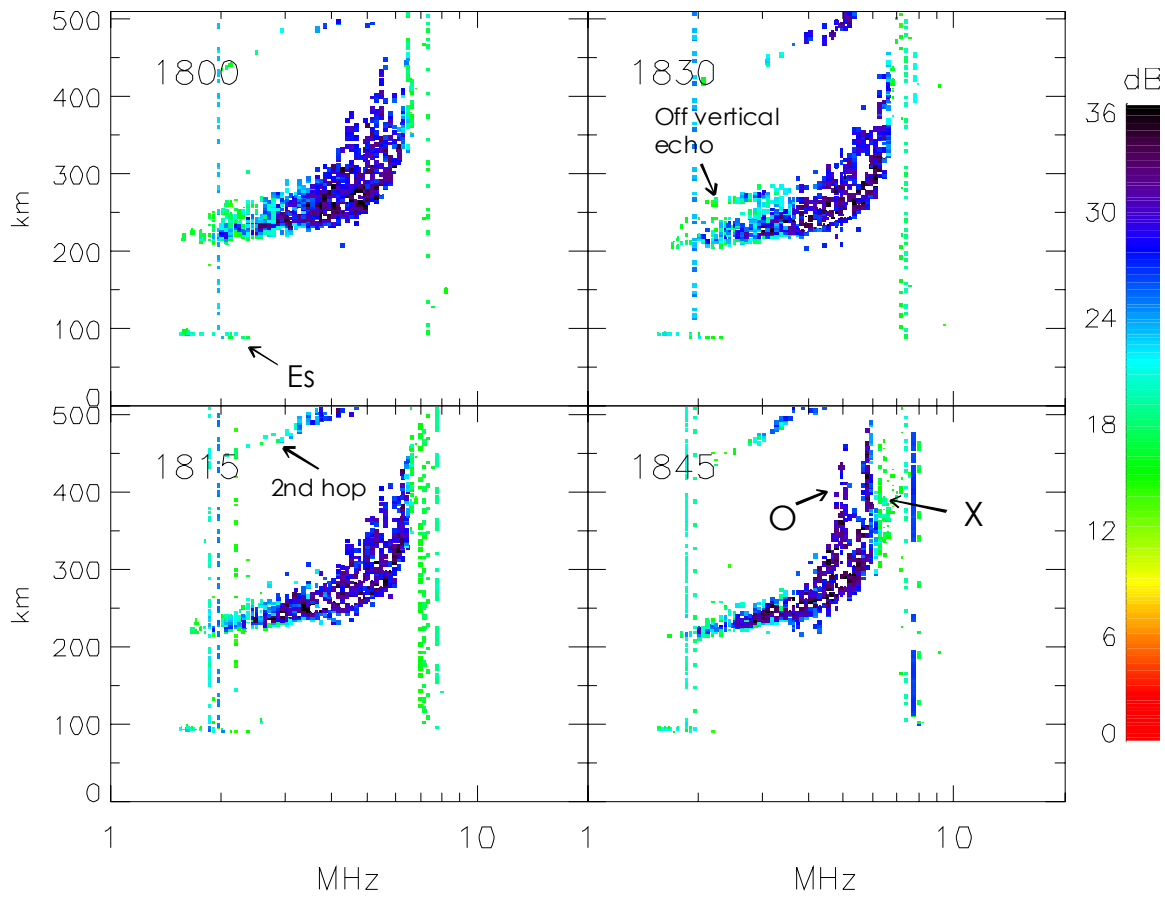

Figure 2-3: Polar Cap Ionograms.

Figure 2-4 shows ionograms from Fortaleza (4°S, 38°W) during daytime 1996 Sept. 13. The F_1 and F_2 layers can be clearly seen (compare with Figure 2-1). The Q-type Sporadic-E marked is a type that is only seen very close to the magnetic dip equator. Another difference between equatorial locations and mid-latitudes is that at the equator the F region is often pushed up to great heights (this sample does not show this) so the height scale needs to go to ~1000 km.

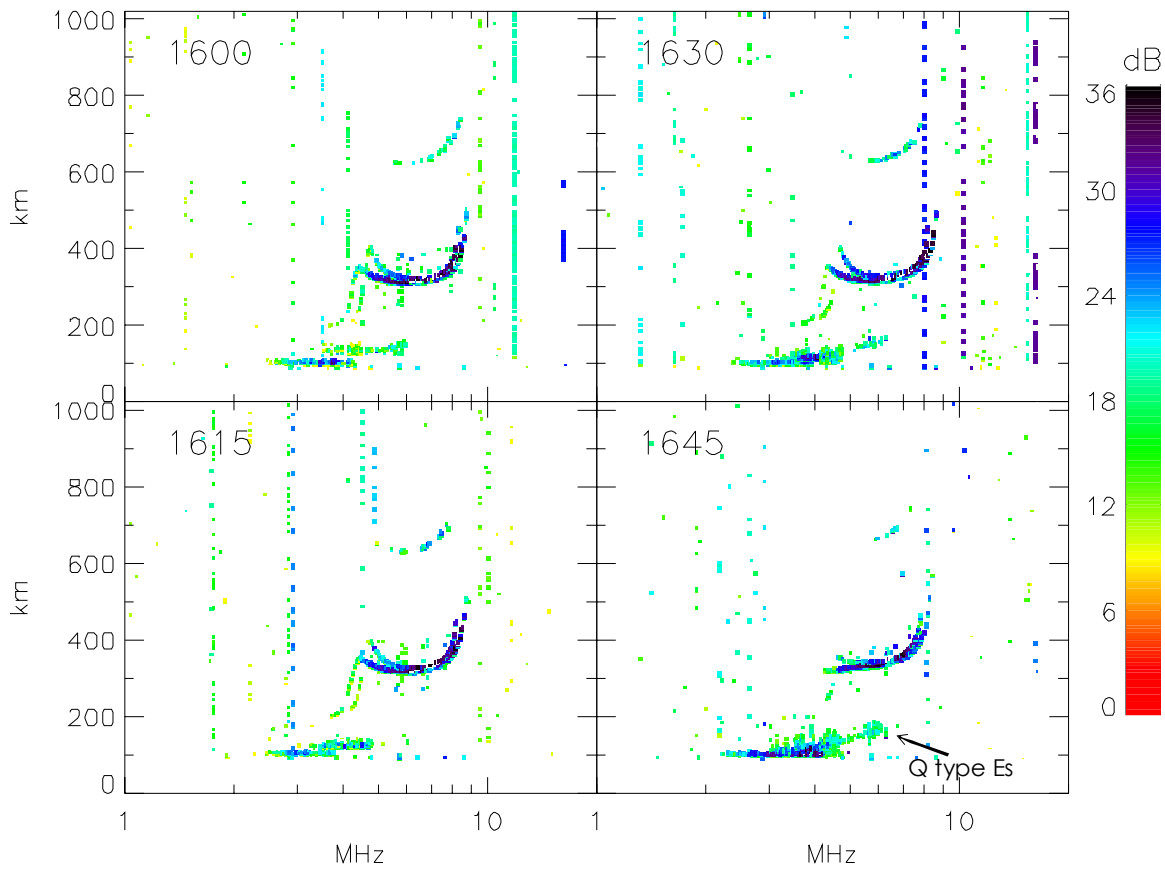

Figure 2-4: Equatorial Ionograms.

2.1.4 Other Ionosonde Measurements

Modern ionosondes usually do a variety of measurements other than just recording ionograms. Some of the additional measurements that are commonly done are discussed here:

- **Oblique Ionograms:** This measurement is used to confirm/determine propagation conditions between two locations. It requires synchronized ionosonde receivers and transmitters at two locations, synchronization now being relatively easy because of GPS. The measurement usually requires the ionosondes used at the two ends of the path to operate on frequencies higher than those used for vertical ionospheric measurements, and requires measurements for longer ranges.
- **Ionospheric Velocities (HF Doppler Technique):** By taking a series of samples and from the series determining the Doppler shifts one can determine the ionospheric velocities. This measurement only works well for giving the ionospheric vector velocity if there are many ionospheric reflecting 'glints'. If there is Spread-F there are normally many glints and therefore the possibility of good ionospheric vector velocities using this technique.
- **Ionospheric Absorption:** Ionosonde data are not commonly analysed for absorption, but usually the echo strengths are recorded so the temporal variation can easily be obtained. Since this method can measure absorption at many HF frequencies it is more sensitive than the usual riometer measurements when absorption is weak.
- **Traveling Ionospheric Disturbances:** TIDs are launched by various atmospheric/ionospheric disturbances, usually atmospheric gravity waves. They usually show up clearly in the F region where they cause variations in ionospheric height and density. To obtain information about the

TID propagation requires the combination of measurements from several separated ionosondes which need to operate at a rate sufficient to measure the TID variations which typically have periods ranging from a few minutes in the E region to tens of minutes in the F region.

Future ionosondes will be improved relative to current models by, in particular, the use of 'software radio' technology which will make it much simpler to build a high quality receiver for HF. This is especially true since at HF the incoming signal, after slight amplification, can be directly digitized. This software radio technology eliminates the 'image' problem in HF receivers. The image problem arises as follows: An ionosonde receiver is required to receive over a range of frequencies, 1 – 20 MHz being typical. In a standard superheterodyne receiver the incoming radio frequency signal is mixed (multiplied) with the local oscillator signal and the frequency difference between the incoming signal and local oscillator is the intermediate frequency, $f_{IF} = f_{RF} - f_{LO}$ or $f_{RF} = f_{LO} + f_{IF}$. Most of the receiver amplification is done in the intermediate frequency amplifier. Now there is a problem in this because it is easily shown that the above equation should actually be $f_{RF} = f_{LO} \pm f_{IF}$ so the receiver can simultaneously receive 2 frequencies. One of these frequencies is the 'correct' RF frequency and the 2nd is the image. Because the receiver has to operate over a range of RF frequencies the image will be a problem unless the IF frequency is selected so that the image frequency is not in the 1-20 MHz band of frequencies. This requires the use of a high IF frequency (>20 MHz) and make for a somewhat convoluted arrangement of intermediate frequency stages in some receivers. In a software radio this problem does not occur because, effectively, one can choose an IF frequency = 0 so there is no image.

As a basic tool for ionospheric monitoring and measurements the ionosonde has been a fundamental instrument for more than 50 years. The modern ionosonde is much cheaper and runs with minimal maintenance as compared to the older ionosondes. The modern ionosonde can also do ancillary measurements, some of which are listed above.

2.1.5 References

Huang, J. and J. MacDougall, Legendre coding for digital ionosonde, Radio Sci. 40 (RS4013), doi: 10.1029/2004RS003123, 2005.

Hunsucker, R. D., Radio Techniques for Probing the Terrestrial Ionosphere, Physics and Chemistry in Space Vol. 22, Springer-Verlag, 1991.

Reinisch, B.W., "Modern Ionosondes", Modern Ionospheric Science, H. Kohl, R. Ruster, and K. Schlegel (eds.), pp. 440-458, 1996.

Titheridge, J. E., Ionogram Analysis with the Generalized Program POLAN, World Data Center A report UAG-93, 1985.

Titheridge, J. E. The real height analysis of ionograms: a generalized formulation. Radio Sci. 23, 831-849, 1998.

2.2 TOPSIDE SOUNDING

(Gordon James, Communications Research Centre)

2.2.1 Introduction

The concept of a topside "ionosonde", or similar, radar on an artificial satellite began to be developed in the late 1950s, not long after the Soviet launch of Sputnik 1. Canada and the U.S.A. agreed to work on fixed- and swept-frequency topside sounders in 1959. The first swept-frequency sounder spacecraft

Alouette-I was launched in 1962, followed by a fixed-frequency sounder on Explorer-20 in 1964. The success of swept-frequency sounding with Alouette-I led to extensive international participation in research on the resulting data. There followed the launching of three more Canada-U.S. sounders: Alouette II, ISIS I, and ISIS II.

The major findings of the Alouette-ISIS scientific program fall mostly into 3 major areas [IEEE, 1969; Jackson et al., 1980]:

1) A wealth of global information has been gathered about the electron density distribution from the F-region electron peak upwards, not obtainable in any other way. Techniques were developed for deconvolving topside sounder ionograms, using cold-plasma and geometric-optics concepts, into profiles of density with altitude that, when combined in continuous series, provided two-dimensional views of the structure of the topside ionosphere, over a range of scale sizes;
2) A variety of short wavelength electrostatic waves requiring hot-plasma concepts and sometimes the consideration of large-signal nonlinearity for their explanation have been documented; and
3) Understanding has been enlarged about the nature of a variety of spontaneous electromagnetic radiations emanating from free-energy sources in space or on the ground.

The mini-review of Jackson et al. [1986] on topside sounding up to the 1980s summarizes the techniques used to obtain topside ionograms and reduce them to electron profiles. The Jackson et al [1986] review is relevant to the present paper in its explanation of the most important differences between satellite-based ionograms and ground-based ionograms described in the previous section.

Sounders were placed on later spacecraft by other national agencies:

1) The ISS-b (Japan – 1978) [Wakai, 1980] sounder data were used to study global F-region distribution of density.
2) The Soviet Interkosmos-19 (1979) and Cosmos -1809 sounders (1986) [Shuiskaya et al., 1990] provided data for research on plasma nonlinearities triggered in the intense near fields of transmitting antennas.

Jackson's [1986] bibliography reported several hundred papers in the archival literature based on Alouette-ISIS data. The story, however, has not ended. The systematic digitization of Alouette and ISIS ionograms and the subsequent use of this accessible data attest to the ongoing relevance of sounder data for modern research subjects [Benson and Osherovich, 2004].

Low-power sounders, also called "relaxation" sounders, have been productive in extending our understanding of electrostatic resonance waves that reflect at short distances from an active spacecraft. The resulting resonance observations were processed into data sets of the spatial dependence of plasma parameters in various regions coverable by Earth-orbiting spacecraft. Examples of these are the French GEOS-1 and -2 [Etcheto et al., 1981], the Japanese EXOS series [Oya and Ono, 1981] and the ESA Cluster [Trotignon et al., 2004].

2.2.2 The Radio Plasma Imager on the IMAGE Spacecraft

In 2000, NASA launched the Radio Plasma Imager (RPI) on the Imager for Magnetopause-to-Aurora Global Exploration (IMAGE) spacecraft. The RPI has been employed for radio sounding from magnetospheric altitudes up to 8 earth radii, relaxation sounding, and passive plasma wave observations [Green and Reinisch, 2003]. A method for determining the density distribution of the plasma from either direct or field-aligned echoes has been applied to the determination of the evolving density structure of the polar cap and the plasmasphere, under a variety of geomagnetic conditions. The RPI plasma resonance observations provide data on the ambient plasma densities and on electrostatic wave resonances at large radial distances. The RPI

long antennas and noise receivers yielded new evidence about the nature of spontaneous continuum radiation and auroral kilometric radiation. Coordination of RPI and the Extreme Ultraviolet (EUV) imager on IMAGE resulted in discoveries about the relation of kilometric continuum to the shape of the plasmasphere. Finally, RPI has been used to successfully test the feasibility of magnetospheric tomography, using intersatellite transmission to the Wind spacecraft.

2.2.3 Future

It seems likely that active ionospheric RF sounding will continue to be pursued. The MARSIS radar on the MARS EXPRESS spacecraft was conceived primarily for surface sounding of that planet but turned up some ionospheric topside signatures that have been interpreted with notions used on the terrestrial sounder observations [Gurnett et al, 2006]. The Enhanced Polar Outflow Probe (ePOP) experiment [Yau et al., 2006] will be launched in 2008 on the Earth-orbiting CASSIOPE spacecraft. CASSIOPE will venture into a new version of transionospheric HF sounding, wherein an ionosonde on the ground will both provide conventional soundings of the bottomside and signals transmitted to CASSIOPE. The resulting observations will be combined for imaging of ionospheric density structure.

2.2.4 References

Benson, R.F. and V.A. Osherovich, Application of ionospheric topside-sounding results to magnetospheric physics and astrophysics, *Radio Science, 39*, RS1S28, doi:10.1029/2002RS002834, 2004.

Etcheto, J., H. de Feraudy, and J.H. Trotignon, Plasma resonance stimulation in space plasmas, *Adv. Space Res, 1*(2), 183-196, 1981.

Green, J.L. and B.W. Reinisch, *Space Science Reviews*, Special issue on IMAGE results, 109, 183-210, 2003.

Gurnett, D. , R. Huff , D. Kirchner, D. Morgan, A. Persoon, T. Averkamp, F. Duru, F. Akalin, E. Nielsen, A. Safaeinili, J. Plaut, and G. Picardi, Mars Express radar soundings of the ionosphere of Mars, COSPAR Scientific Assembly 2006, Beijing, 16-23 July, Paper C3.2-0007-06, 2006.

IEEE, Special issue on topside sounding and the ionosphere, *Proc. IEEE*, *57*, 6, 1969.

Jackson, J.E., E.R. Schmerling, and J.H. Whitteker, "Mini-review on topside sounding," *IEEE Trans. Ant. Propag., 28*(2), 284-288, 1980.

Jackson, J.E., Alouette-ISIS program summary, National Space Science Data Center, Doc. no. NSSDC/WDC-A-R&S 86-09, Greenbelt, MD, U.S.A., 1986.

Oya, H. and T. Ono, Stimulation of plasma waves in the magnetosphere using satellite Jikiken /EXOS-B/, *Adv. Space Res., 1*(2), 217-220, 1981.

Shuiskaya, F.K., Yu. I. Galperin, A.A., Serov, N.V. Baranets, Yu.V. Kushnerevsky, G.V. Vasil'ev, S.A. Pulinets, M.D. Fligel and V.V. Selegey, Resonant heating of the ionospheric plasma by powerful radiopulses aboard the Intercosmos-19 and Cosmos-1809 satellites, *Planet. Space Sci.*, *38*(2), 173-180, 1990.

Trotignon, J.G., P. M. E. Décréau, J. L. Rauch, E. Le Guirriec, P. Canu, and F. Darrouzet. The Whisper Relaxation Sounder Onboard Cluster: A Powerful Tool for Space Plasma Diagnosis around the Earth, *Cosmic Res. 41*(4), 345-3348, 2004.

Wakai, N., "Operation and experimental results of the Ionosphere sounding satellite ISS-b", *Acta Astronautica, 7*, 999-1020, 1980.

Yau, A.W., H.G. James and W. Liu, The Canadian Enhanced Polar Outflow Probe. (e-POP) Mission in ILWS, *Advances in Space Research*, *38*(8), 1870-1877, DOI:10.1016/j.asr.2005.01.058, 2006.

2.3 THE SUPERDARN RADAR NETWORK

(William A. Bristow, Geophysical Institute University of Alaska Fairbanks)

The Super Dual Auroral Radar Network, SuperDARN, [Greenwald *et al*., 1995] is the product of more than twenty years of research and development which began in 1983 with the construction of an HF radar at Goose Bay, Labrador. In the intervening years, the HF radar technique has had a major impact on high-latitude ionospheric research in both the aeronomy and magnetospheric physics communities. During that time, SuperDARN has evolved from a single independent radar to a network of ten operational radars in the northern hemisphere and seven operational radars in the southern hemisphere. A plan view of the current coverage of the northern network is shown in Figure 2-5. With the addition of the Alaskan radars in 2000 and 2001, there is continuous SuperDARN coverage extending form northern Scandinavia westward to Siberia with extensive conjugate coverage in the southern hemisphere. In the standard mode of operation, each radar measures the line-of-sight plasma velocity at 75 ranges along each of 16 beam directions covering an area of about 3500 km in range and about 56 degrees in azimuth. The radars operate continuously, 24 hours per day and 7 days per week and deliver images of the high-latitude convection pattern with a one to two-minute time resolution.

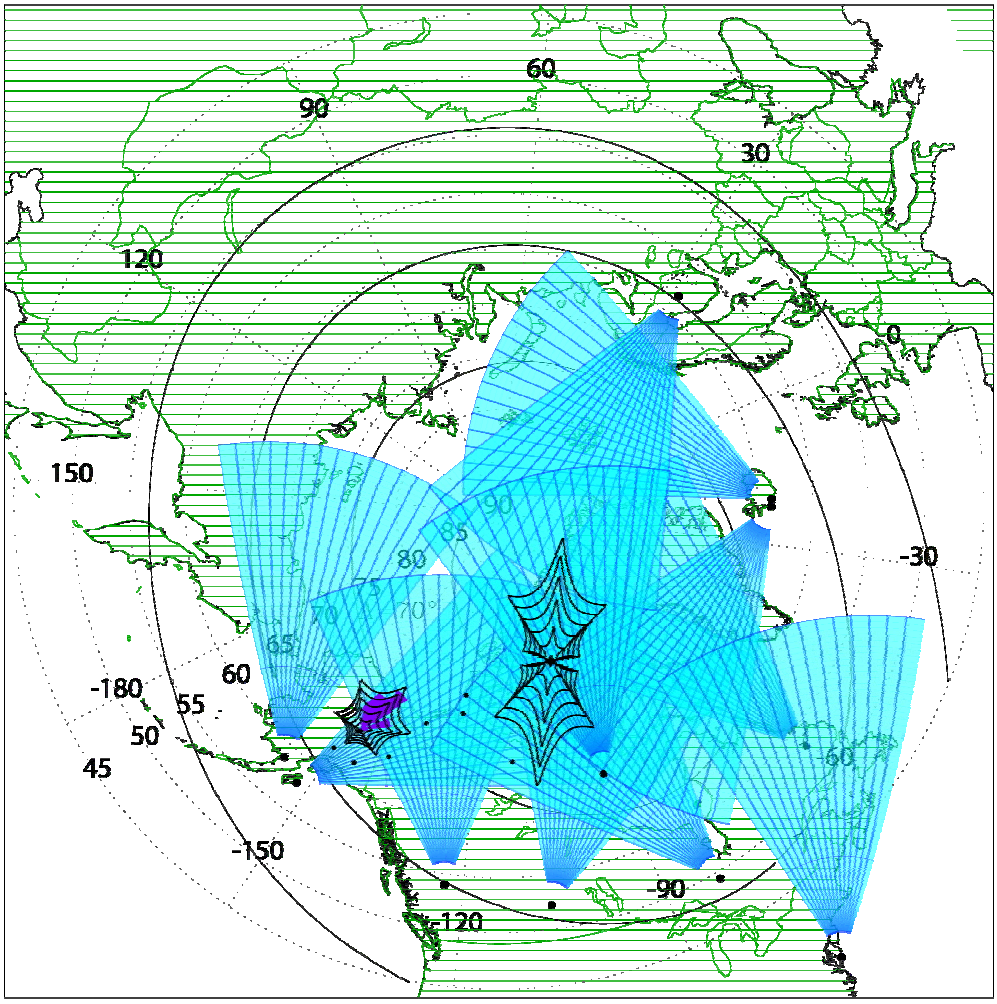

Figure 2-5: Fields of View of the Northern SuperDARN Radars.

The main purpose of SuperDARN is the instantaneous mapping of the ionospheric convection pattern. By providing direct measurements of convection velocities over large regions, SuperDARN provides the best means available to derive ionospheric convection patterns. Prior to the development of SuperDARN, our knowledge of convection was based primarily upon conceptual models, simulations, and empirical models that were developed from observations accumulated over time. Convection data that have been available include: single point radar observations of plasma flows, low altitude satellite observations of plasma drifts, high-altitude satellite observations of electric fields, and observations of magnetic perturbations by satellite-based and ground-based magnetometers. Each of the previously available techniques has characteristics that may cause the derived pattern to differ from the actual pattern at any given moment. SuperDARN provides direct, instantaneous, measurement of convection and hence, avoids many of the drawbacks of other techniques.

Each radar consists of a phased-array antenna system, sixteen transmitters, a receiver, a phasing matrix, and a computer system for control and data logging. The antenna system consists of two rows of log periodic antennas covering the frequency range from 8 MHz to 20 MHz. One row, of sixteen antennas, is used for transmission and reception, the second row, of four antennas, is used for reception only. Both arrays are steered into sixteen viewing directions by an electronic phasing matrix. The two rows of antennas are separated along their array normal direction and are used as an interferometer to derive angle-of-arrival information from the received signals.

Data from the network can be accessed in real time through the SuperDARN page. Follow real-time data link and then the Java applet link and read the instructions on how to view the data. Figure 2-6 is an example display from the Kodiak radar. This image is from about 1830 UT on January 27, 2000. It was a relatively active interval when Alaska was in the dawn sector. The gray region represents the ground-scattered portion of the signal, that is, signal that is transmitted from the radar, reflects obliquely off of the lower portion of the F-region ionosphere down to the ground where it scatters back along the same path to the radar. The ground scatter is useful for obtaining the density structure of the bottom-side F-region. The colored regions represent scatter from decameter-scale plasma irregularities. These irregularities are in the F-region and move with the bulk plasma velocity. The color scale corresponds to the component of the plasma velocity along the radar line of site. The red and yellow colors correspond to velocity away from the radar, while blue colors correspond to velocity toward the radar.

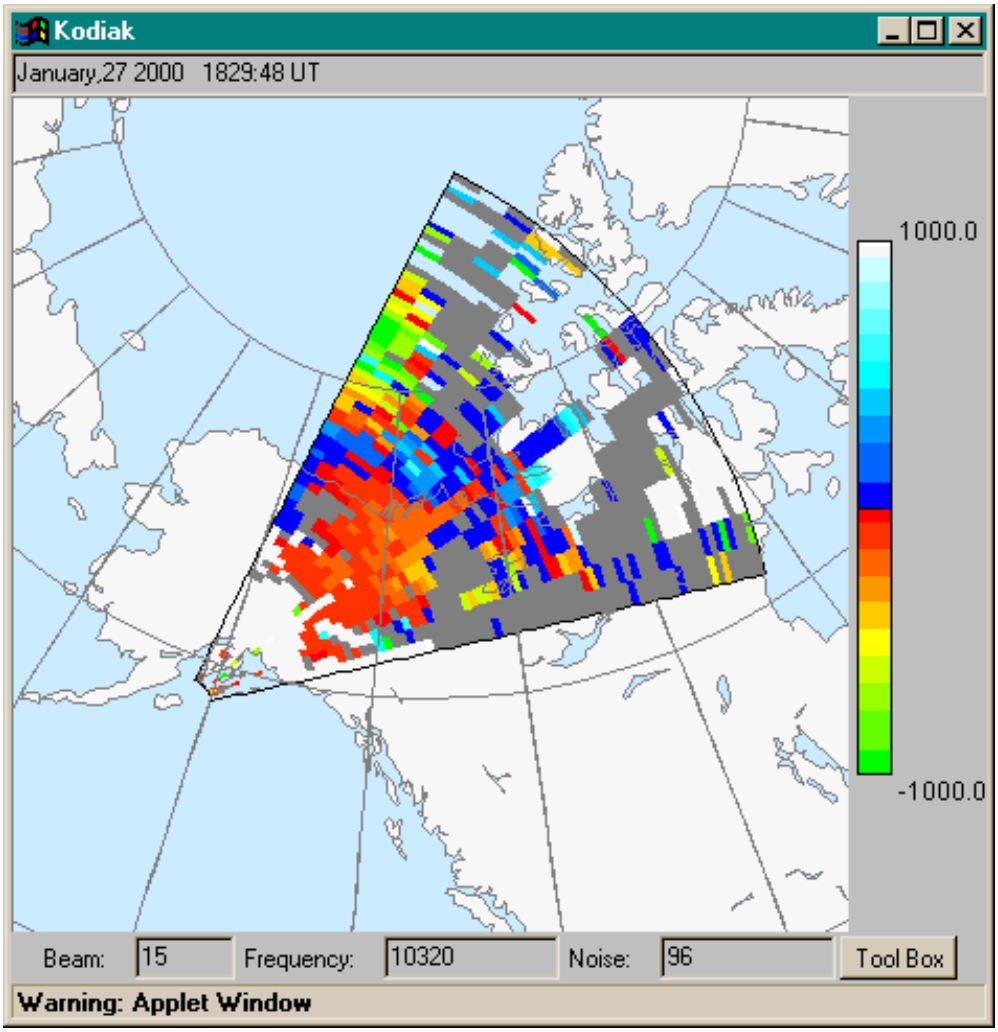

Figure 2-6: Example of Velocity Observations from the Kodiak SuperDARN Radar.

In addition, the data are being assimilated into the northern-hemisphere convection mapping, which also can be viewed through the real-time data link. Below is and example convection map from the same interval as the above image of the Kodiak field of view.

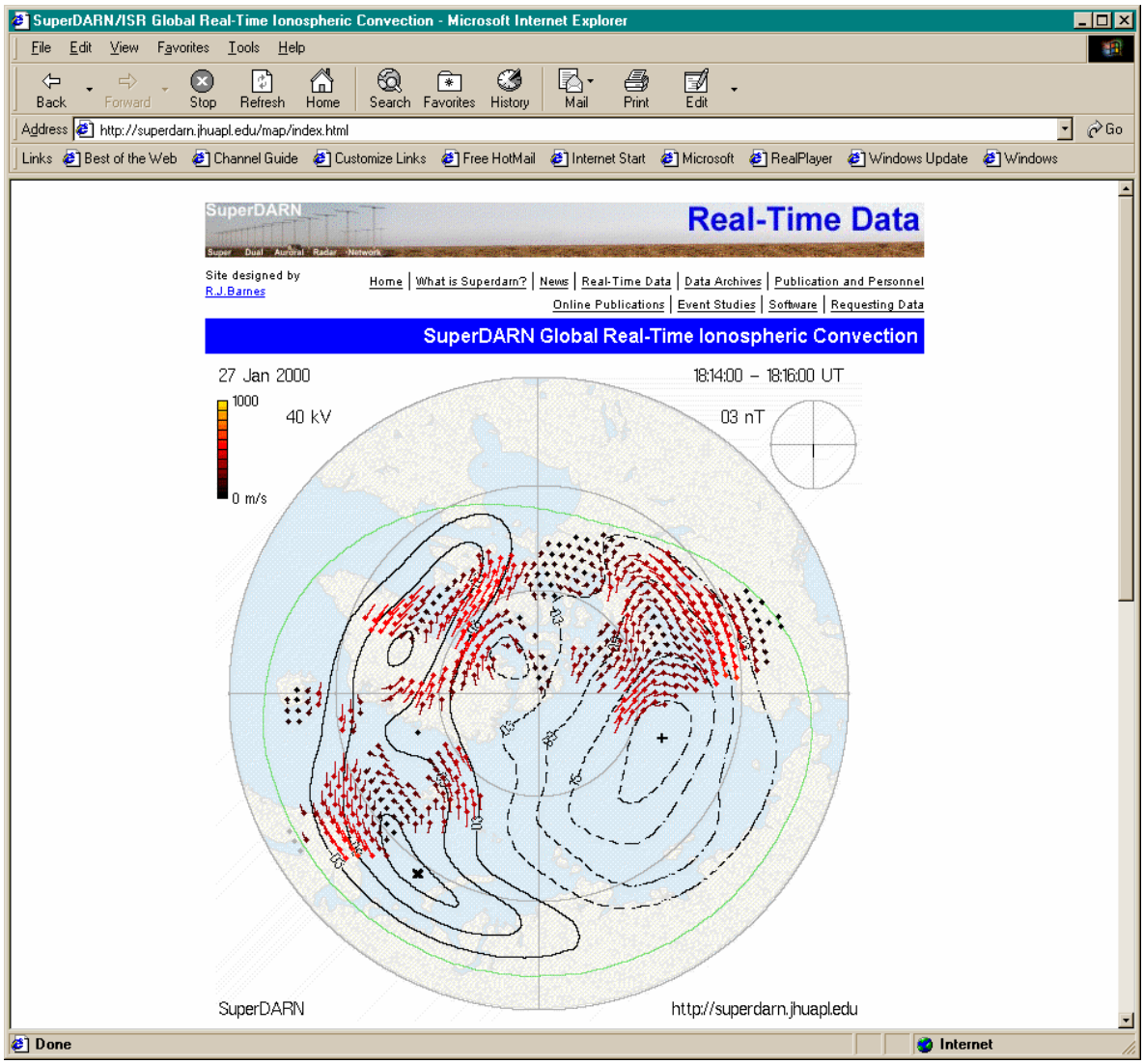

Figure 2-7: Example Convection Pattern from the Real-Time Display on the JHUAPL Web Page.

In addition to convection pattern measurements, SuperDARN has been used for many other types of observations. A listing of publications that rely on data from SuperDARN can be found on the SuperDARN web page at the Johns Hopkins University Applied Physics Laboratory: http://superdarn.jhuapl.edu.

Radio propagation over Alaska is one example of studies enabled by SuperDARN. The work carried out in this area has resulted in development of a measurement technique for estimating HF communication parameters [Hughes et al, 2002], which has had the side benefit of improving operation of the network. The principle used for estimating HF communications parameters with an HF radar is simple. Under common conditions, a portion of the signal transmitted from the radar reflects from the ionosphere towards the ground. Upon striking the ground, some of the signal is scattered back in the direction from which it was incident and returns to the radar. This signal is termed ground scatter, and is easily distinguished from the scatter from ionospheric plasma irregularities. Reflection of a ray from the ionosphere depends on the ionospheric plasma density, the frequency of the signal, and the angle of incidence of the ray. By determining the critical angle below which reflection occurs as a function of frequency, it is possible to map the F-region critical frequency for vertical incidence (f_oF_2), which directly translates to the peak plasma density. The experiment technique developed for this observation used spare

time available in the normal SuperDARN measurement cycle to rapidly step through frequencies and observe the ground scatter. This technique provides estimates of the F-region peak density over a range of distances along each beam direction of the radar. Figure 2-8 shows a map of these f_oF_2 observations. The technique has the side benefit that while observing ground scatter, it is also possible to determine the optimum frequency for observing ionospheric scatter. A second algorithm exploits this to automatically select the radar operating frequency, which has resulted in a great increase in the amount of ionospheric scatter observed by the radars.

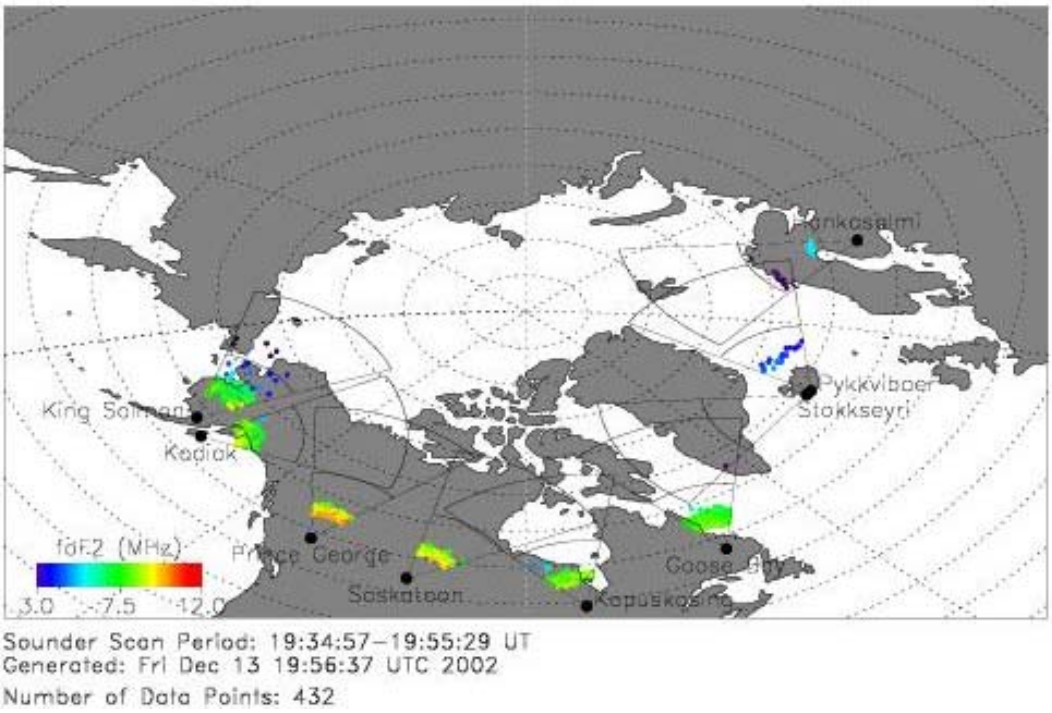

Figure 2-8: f_oF_2 Estimates from the SuperDARN Network.

SuperDARN Contributions to the HAARP/HIPAS programs have been significant. Primarily, work has focused on HAARP, which is a DOD operated facility for radio frequency heating of the ionospheric plasma. In heating the plasma, various instabilities generate plasma irregularities similar in character to the naturally occurring irregularities, which are the primary target of the Kodiak radar. Because the artificial irregularities reliably generate strong scatter, the radar has become one of the primary diagnostics for HAARP heating experiments. The radar at Kodiak and the group at UAF have supported every HAARP experiment campaign since the radar was completed. The primary focus of the UAF group has been determining the characteristics of the irregularities including their formation time, decay time, threshold for generation, effect of the angle between the RF heating signal and the Earth's magnetic field, and the frequency of the heating signal. Recently, installation of a digital receiver enabled experiments to search for reflections from various other plasma wave modes. The search was indeed successful. A variety of lines were observed in the reflection spectrum with frequencies that were related to the gyro-harmonics and other characteristic plasma frequencies. One segment of the signals had distinct characteristics that could be identified as scatter from upper-hybrid waves. These never before reported observations resulted in two manuscripts [Hughes et al, 2003; Hughes et al., 2004], and will be the seeds for much further research.

In the studies of magnetospheric field-aligned currents, global-scale convection data from the SuperDARN network were combined with ionospheric conductance patterns estimated from ultraviolet images of

auroral emissions observed by the Polar Ultra Violet Imager (UVI). Conductance estimates were determined by observing the intensities and the ratio of the upper and lower Lymon-Birge-Hopfield bands. Polar UVI provided these images with about a 1-minute cadence during some periods, which allowed studies of the simultaneously evolving conductance and convection patterns. Combining the conductance and the convection provided estimates of the currents flowing perpendicular to the Earth's magnetic field from which it is possible to infer the field-aligned currents by realizing that in regions where the perpendicular currents diverge, currents must flow along the magnetic field. These field-aligned currents are the primary mechanism by which energy flows from the magnetosphere into the ionosphere and upper atmosphere. The Bristow et al. [2001] study examined the evolution of currents in the high-latitude and polar regions as solar-wind conditions changed and during one substorm period. The strongest currents observed in the day side were transients in the cusp region, while on the night side, strong currents were observed to follow the head of the substorm expansion bulge.

Observing substorm convection using SuperDARN was a direct follow on to the field-aligned current studies. Again, observations from Polar UVI were combined with convection observations, with the addition of ground-based magnetometer observations, and observations from all-sky imagers and meridian scanning photometers. A number of substorm intervals were examined to determine general characteristics in the relationship between the plasma flow, the optical emissions, and the currents. In the initial study [Bristow et al., 2001] it was found that the global-scale convection pattern evolved steadily in the substorm growth phase to enhance the shear in the pre-midnight convection resulting in evolution of what magnetometers observe as the Harang discontinuity. The discontinuity moved to lower latitudes as the shear increased, and extended across the midnight meridian. After a period of time, zonal convection near midnight was observed to increase rapidly to high velocities. Then, as the auroral emissions increased, the convection velocity decreased, the shear in the pattern decreased, and flow near midnight rotated from zonal to nearly meridional out of the polar cap. The second study [Bristow et al., 2003] focused on the detailed evolution and sequence of events during the late growth phase and expansion phase of substorms.

A definite sequence of events was identified in which the first evidence of expansion was a surge of convection, followed by an increase in auroral luminosity, and finally followed by the negative magnetometer bay that is often used to identify substorms. In addition, it demonstrated that there was no evidence for magnetic merging until the time of the negative magnetometer bay. The magnetometer bay also coincided with relaxation of the convection shear, and rotation of flow to being directed out of the polar cap. Figure 2-9 illustrates the merging of the radar data with ground-based all-sky imager observations of the aurora. The correspondence between the observed sheer in the flow with the location of auroral arcs is phenomenal.

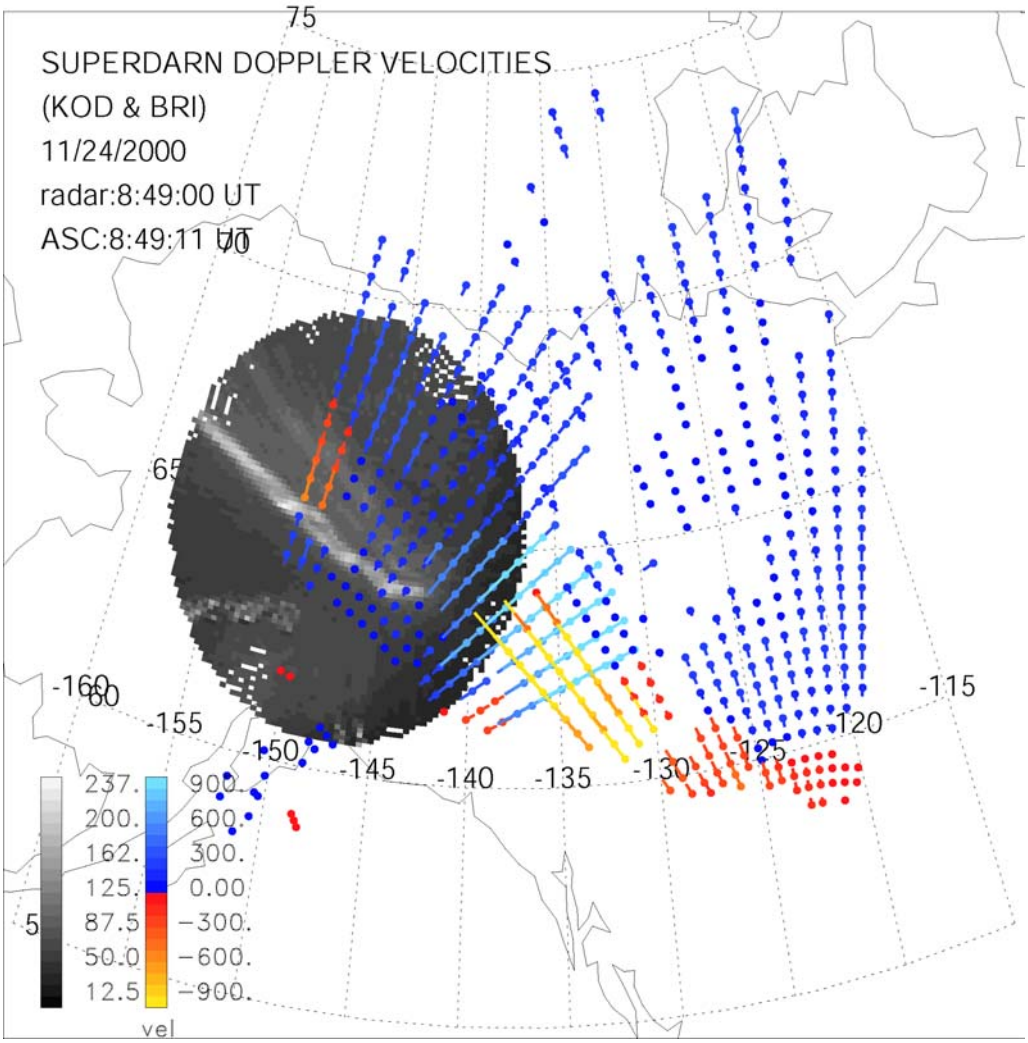

Figure 2-9: Superposed Plasma Velocity Observations and Auroral Luminosity Observations.

All of the topics discussed so far relate to properties of the ionospheric plasma, or use reflections from the ionospheric plasma to observe magnetospheric phenomena. In addition to these topics, the SuperDARN group has exploited scatter from ablating meteors to observe properties of the neutral atmosphere winds in the mesosphere. During the interval reported here, two masters' theses [Wei, 2000; Parris, 2003] have reported various aspects of this topic. Wei [2000] developed an algorithm to separate meteor scatter from other types of scatter in the SuperDARN data set. He was able to examine mesospheric winds at an assumed altitude of about 95 km, and was able to extract the various tidal modes and planetary waves at polar latitudes, and carry out a preliminary analysis of their seasonal behavior. Parris [2003] carried these investigations further and developed an experimental technique for extracting the meteor scatter as a function of altitude. This required replacing the analog receiver at Kodiak with a digital receiver that allowed over sampling of the received signal and multiple data channels. Having multiple channels resulted in two different data streams, which allowed the over-sampled data to be independent of the normal SuperDARN data. The nature of the meteor signal allows treatment as a hard target, providing greater spatial resolution from long duration signals. Exploiting this has provided altitude profiles in the range from about 70 km altitude to about 110 km altitude.

2.3.1 References

Bristow, W. A., D. Lummerzheim, Determination of field-aligned currents using the Super Dual Auroral Radar Network and the UVI ultraviolet imager, J. Geophys. Res. 106, 18,577-18,588, 2001.

Bristow, W. A., A. Otto, and D. Lummerzheim, Substorm convection patterns observed by the Super Dual Auroral Radar network, J. Geophys. Res. 106, 24,593-24,609, 2001.

Bristow, W. A., G. J. Sofko, H. C. Stenbaek-Nielsen, S. Wei, D. Lummerzheim, A. Otto, Detailed analysis of substorm observations using SuperDARN, UVI, ground-based magnetometers, and all-sky imagers, J. Geophys. Res. 108, A3, 1124, doi:10.1029/2002JA009242, 2003.

Greenwald, R. A., et al., DARN/SuperDARN: A global view of high-latitude convection, Space Sci. Rev., 71, 763-796, 1995.

Hughes, J. M., W. A. Bristow, R. A. Greenwald, R. J. Barnes, Determining characteristics of HF communications links using SuperDARN, Ann. Geophys., 20, 1023-1030, 2002.

Hughes, J. M., W. A. Bristow, R. T. Parris, E. Lundell, SuperDARN observations of ionospheric heater-induced upper hybrid waves, Geophys. Res. Lett., 30, doi:10.129/2003GL018772, 2003.

Hughes, J. M.; Bristow, W. A.; Parris, R. T. SuperDARN observations of spectral enhancements excited during an ionospheric heating experiment, Geophys. Res. Lett., Vol. 31, No. 8, L08808 10.1029/ 2004GL019613, 2004.

Parris, R. T., Design and implementation of a meteor tracking retrofit system for the HF radar at Kodiak Island, Alaska, Unpublished M.S. EE thesis, University of Alaska Fairbanks, 2003.

Wei, D., Meteor Wind Wave Analysis of SuperDARN Observations, Unpublished M.S. EE thesis, University of Alaska Fairbanks, 2000.